The Astrophysical Journal, 742:108 (9pp), 2011 December 1 doi:10.1088/0004-637X/742/2/108

PROBING THE STAR FORMATION HISTORY AND INITIAL MASS FUNCTION OF THE $z \sim 2.5$ LENSED GALAXY SMM J163554.2+661225 WITH *HERSCHEL*[*]

Keely D. Finkelstein[1,2], Casey Papovich[1], Steven L. Finkelstein[1,2,7], Christopher N. A. Willmer[3], Jane R. Rigby[4], Gregory Rudnick[5], Eiichi Egami[3], Marcia Rieke[3], and J.-D. T. Smith[6]
[1] George P. and Cynthia Woods Mitchell Institute for Fundamental Physics and Astronomy, Department of Physics and Astronomy, Texas A&M University, College Station, TX 77843-4242, USA
[2] Department of Astronomy and McDonald Observatory, University of Texas at Austin, 1 University Station C1400, Austin, TX 78712, USA
[3] Steward Observatory, University of Arizona, 933 N. Cherry Ave., Tucson, AZ 85721, USA
[4] NASA Goddard Space Flight Center, Code 665, Greenbelt, MD 20771, USA
[5] Department of Physics and Astronomy, 1251 Wescoe Hall Dr., University of Kansas, Lawrence, KS 66045-7582, USA
[6] Ritter Observatory, Department of Physics and Astronomy, University of Toledo, MS 113, Toledo, OH 43606, USA
Received 2011 May 17; accepted 2011 October 13; published 2011 November 14

ABSTRACT

We present the analysis of *Herschel* Spectral and Photometric Imaging Receiver far-infrared (FIR) observations of the $z = 2.515$ lensed galaxy SMM J163554.2+661225. Combining new 250, 350, and 500 μm observations with existing data, we make an improved fit to the FIR spectral energy distribution of this galaxy. We find a total infrared (IR) luminosity of $L(8\text{–}1000\ \mu\text{m}) = 6.9 \pm 0.6 \times 10^{11}\ L_{\odot}$, a factor of three more precise over previous $L_{\rm IR}$ estimates for this galaxy, and one of the most accurate measurements for any galaxy at these redshifts. This FIR luminosity implies an unlensed star formation rate (SFR) for this galaxy of $119 \pm 10\ M_{\odot}\ \text{yr}^{-1}$, which is a factor of 1.9 ± 0.35 lower than the SFR derived from the nebular Paα emission line (a 2.5σ discrepancy). Both SFR indicators assume an identical Salpeter initial mass function (IMF) with slope $\Gamma = 2.35$ over a mass range of 0.1–100 $M_{\odot}$; thus this discrepancy suggests that more ionizing photons may be necessary to account for the higher Paα-derived SFR. We examine a number of scenarios and find that the observations can be explained with a varying star formation history (SFH) due to an increasing SFR, paired with a slight flattening of the IMF. If the SFR is constant in time, then larger changes need to be made to the IMF by either increasing the upper mass cutoff to $\sim$200 $M_{\odot}$, or a flattening of the IMF slope to 1.9 ± 0.15, or a combination of the two. These scenarios result in up to double the number of stars with masses above 20 $M_{\odot}$, which produce the requisite increase in ionizing photons over a Salpeter IMF with a constant SFH.

Key words: galaxies: high-redshift – galaxies: individual (SMM J163554.2+661225) – galaxies: starburst – infrared: galaxies

Online-only material: color figures

1. INTRODUCTION

The recent launch of the *Herschel Space Observatory* (Pilbratt et al. 2010) has opened the high-redshift universe to detailed far-infrared (FIR) investigations. *Herschel* observations of galaxies are specifically useful as they constrain the peak of the FIR spectral energy distributions (SEDs) for $z \sim 2$ galaxies, allowing robust measurements of the total infrared (IR) luminosity, $L_{\rm IR} = L(8\text{–}1000\ \mu\text{m})$, and dust temperature (e.g., Amblard et al. 2010; Elbaz et al. 2010; Magdis et al. 2010). From the total IR luminosity one can infer the star formation rate (SFR) and compare to SFRs based on other indicators. Both $L_{\rm IR}$ and the dust temperature allow for detailed physical investigations of star-forming galaxies not possible without FIR observations.

One important factor for understanding star-forming galaxies at high redshift is the form of the initial mass function (IMF), specifically at the high-mass end. There is currently an ongoing debate as to whether the IMF is universal. In nearby galaxies the IMF is well fitted by a Salpeter (1955) IMF, where $dN/dM \propto M^{-\Gamma}$, with slope $\Gamma = 2.35$ (Elmegreen 2006, and references therein), or even steeper ($\Gamma > 2.35$) in a few examples, such as in regions of the Large Magellanic Cloud (Gouliermis et al. 2005) and low surface brightness galaxies (Lee et al. 2004). On the other hand, the summed IMF in clusters of galaxies appears to be Salpeter or slightly flatter ($\Gamma < 2.35$) than Salpeter (e.g., Renzini et al. 1993; Lowenstein & Mushotzky 1996). Similarly, Baldry & Glazebrook (2003) find that a slightly flatter IMF slope of $\Gamma = 2.15$ is favored to fit the star formation history (SFH) and luminosity density in low-redshift star-forming galaxies. Other evidence for a non-Salpeter IMF is shown by varying the IMF slope or extending the IMF upper mass limit up to at least 120 $M_{\odot}$ over the typical values of 100 $M_{\odot}$ in order to reproduce the observed Hα equivalent widths in Sloan Digital Sky Survey (SDSS) galaxies (Hoversten & Glazebrook 2008, 2011). Additionally, large Lyα equivalent widths in some Lyα-emitting galaxies have been observed which cannot be explained by normal stellar populations, but may be caused by a top-heavy (i.e., flatter) IMF slope (e.g., Kudritzki et al. 2000; Malhotra & Rhoads 2002; Finkelstein et al. 2007).

One way to study the IMF is to compare SFR indicators based on nebular lines, whose luminosities are proportional to the number of ionizing photons generated primarily by O stars, to those based on $L_{\rm IR}$. In a dusty starburst most of the ionizing radiation is absorbed by dust and reprocessed into the thermal infrared, characterized by $L_{\rm IR}$, where $L_{\rm IR}$ is expected to be proportional to the bolometric luminosity ($L_{\rm bol}$; Kennicutt 1998). While *Herschel* can permit direct measurements of $L_{\rm IR}$, the majority of galaxies at cosmological

[*] *Herschel* is an ESA space observatory with science instruments provided by European-led Principal Investigator consortia and with important participation from NASA.
[7] Hubble Fellow.

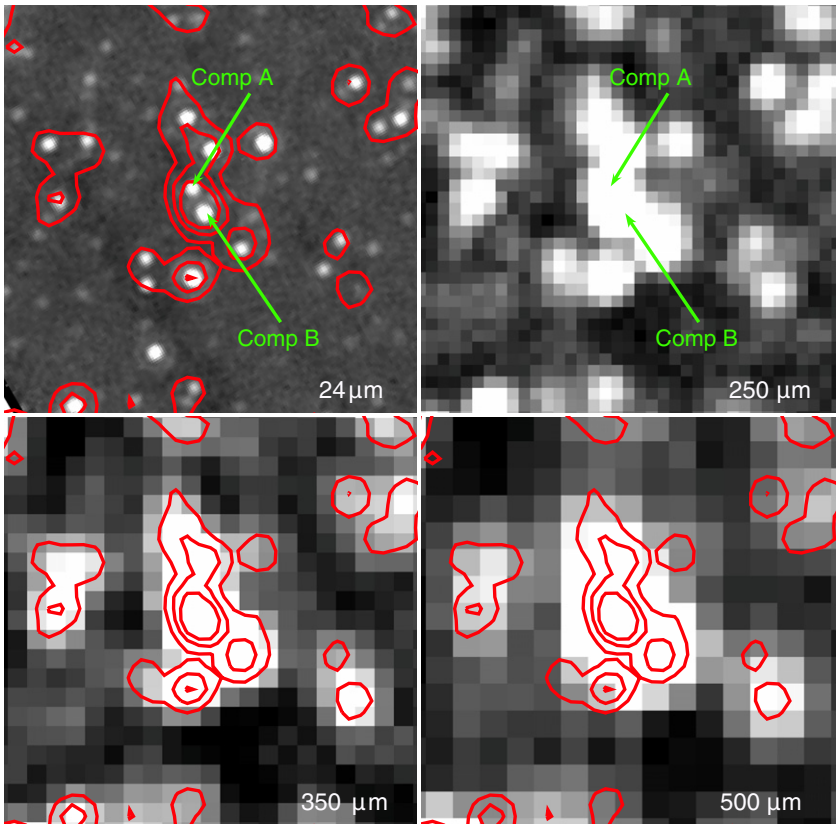

Figure 1. Mid- and far-IR images of the lensed galaxy SMM J163554.2+661225. The four panels show 215″ × 215″ regions around the two dominant lensed components (A and B, as labeled) in the *Spitzer* MIPS 24 and *Herschel* SPIRE 250, 350, and 500 μm data (as labeled). The contours show levels 1σ, 3σ, and 5σ above the noise per pixel in the 250 μm data. While the 24 μm data resolve components A and B of SMM J163554.1+661225, these components are blended in the *Herschel* SPIRE data. Accordingly, we fit the *Herschel* data with GALFIT using the positions of components A and B from the 24 μm image.

(A color version of this figure is available in the online journal.)

distances fall well below the 5σ confusion limit of 25–35 mJy for *Herschel* at 250–500 μm (e.g., Chapman et al. 2002; Kneib et al. 2004). Fortunately, gravitationally lensed systems can easily be observed in the submillimeter by *Herschel* and other submillimeter telescopes. One such galaxy is SMM J163554.2+661225 at $z = 2.515$, which is gravitationally lensed by the rich cluster Abell 2218 (Kneib et al. 2004). The system was first discovered in the submillimeter at 450 and 850 μm by SCUBA on the James Clerk Maxwell Telescope (Kneib et al. 2004) as a multiply lensed system. The brightest component (component B) has a lensing magnification of 22 and the second brightest component (component A) has a lensing magnification of 14 (Kneib et al. 2004). SMM J163554.2+661225 was observed by Rigby et al. (2008) in the mid-IR with *Spitzer* from 3.6 to 8.0 μm with the Infrared Array Camera (IRAC; Fazio et al. 2004), at 24–160 μm with the Multiband Imaging Photometry for *Spitzer* (MIPS; Rieke et al. 2004), and with the *Spitzer* Infrared Spectrograph (IRS; Houck et al. 2004). Papovich et al. (2009, hereafter P09) also analyzed mid-IR *Spitzer* IRS spectroscopy of component B to make the first detection of Paα emission in a high-redshift galaxy, from which they derived a revised dust-corrected Paα SFR of 225 $\pm$ 37 $M_\odot$ yr^{-1} for a Salpeter IMF with upper and lower mass cutoffs of 100 $M_\odot$ and 0.1 $M_\odot$, respectively.

In this paper, we present new *Herschel* Spectral and Photometric Imaging Receiver (SPIRE; Griffin et al. 2010) observations of SMM J163554.2+661225. In Section 2, we analyze the SPIRE data, including the measurement of crowding-corrected flux densities. In Section 3, we derive the rest-frame FIR luminosity, dust temperature, and IR SFR. We compare these results to local samples and other high-redshift submillimeter galaxies (SMGs). In Section 4, we discuss the implications of the variations in SFRs on the SFH and IMF. In Section 5, we present our summary and conclusions. Where applicable, we use a cosmology with $H_0 = 70$ km s^{-1} Mpc^{-1}, $\Omega_m = 0.3$, and $\Omega_\lambda = 0.7$.

2. DATA ANALYSIS

Herschel SPIRE 250, 350, and 500 μm data of Abell 2218 were taken as part of the *Herschel* Multi-tiered Extragalactic Survey (HerMES; Oliver et al. 2010). The reduced SPIRE data of Abell 2218 were accessed through the HeDaM database[8] and were processed using the *Herschel* Interactive Pipeline Environment (HIPE v2.3) as described in Oliver et al. (2010). The SPIRE 250, 350, and 500 μm images are blended for the two components (A and B, see Figure 1) of the lensed galaxy SMM J163554.2+661225. We used the galaxy-fitting software GALFIT (v3.0; Peng et al. 2010) to perform point-source function (PSF) fitting of the SPIRE data for the two components of the galaxy. Figure 1 shows a 215″ × 215″ region around SMM J163554.2+661225 in *Spitzer* MIPS 24 μm, and the SPIRE 250, 350, and 500 μm data, with 250 μm contours overlaid on the other images. We used the positions of the two components from the MIPS 24 μm image as a prior for the location of the components in the SPIRE 250 μm image. We

[8] http://hedam.oamp.fr

Table 1
SPIRE Flux Density Measurements for Component B[a]

Wavelength (μm)	Flux Density (mJy)	Measured Error (mJy)	Confusion Error[b] (mJy)	Total Quadrature Summed Error[c] (mJy)
250	55.5	2	5.8	6.1
350	56	7	6.5	9.4
500	34	8	7.3	10.5

Notes.
[a] Photometry for component A is approximately 1.5 times fainter.
[b] Nguyen et al. (2010).
[c] These total errors do not include an additional 15% error based on SPIRE's estimated absolute calibration uncertainty (Griffin et al. 2010).

ran Source Extractor (Bertin & Arnouts 1996) on the SPIRE images prior to GALFIT to estimate input magnitudes, radial profile, and positions of other sources in the image. GALFIT was run on each of the SPIRE images on a $215'' \times 215''$ region centered on the two dominant lensed components, fitting all sources. GALFIT requires both an uncertainty image and a PSF. The uncertainty images from the *Herschel* archive for this field were used and we adopted the *Herschel*/SPIRE theoretical PSFs.[9] The SPIRE 250, 350, and 500 μm beams are Gaussian with full width at half-maximum values of $18.''1$, $25.''2$, and $36.''6$, respectively. We also compared the results using model PSFs from the GOODS/*Herschel* survey (PI: D. Elbaz). The flux density measurements varied by less than 5% based on the choice of PSF.

The components of the lensed galaxy are reasonably resolved in the 250 μm image (see Figure 1). Therefore, we measured the flux density for each source in the 250 μm image using GALFIT, and allowing the position to vary within the 1σ positional uncertainty from SExtractor with no other constraints. We measure a flux density at 250 μm for component B (the brightest component), $S_{250} = 55.5 \pm 2$ mJy. The measured flux density ratio between the two components is $S_{250}(\mathrm{B})/S_{250}(\mathrm{A}) = 1.5 \pm 0.1$. This ratio is consistent with the flux density ratio measured at 24 μm from P09, $S_{24}(\mathrm{B})/S_{24}(\mathrm{A}) = 1.6$, where the 24 μm flux densities of components A and B are 0.72 mJy and 1.16 mJy, respectively. This flux density ratio is also consistent with the reported ratios of components B and A at 450 and 850 μm (Kneib et al. 2004).

The A and B components of this lensed galaxy are more severely blended in the longer wavelength SPIRE 350 and 500 μm data (see Figure 1). Therefore, we add a priori constraints on both the astrometric positions and flux density ratio to extract the individual flux densities. We measured flux densities for the components by fixing the positions of each component to have the value measured in the 250 μm image. We also include a constraint that the flux density ratio at 350 and 500 μm for the two components has the same ratio measured at 250 μm. Given the uniformity in the flux density ratios of the A and B components from the mid-IR (24 μm), far-IR (250 μm), and submillimeter (450–850 μm) (see paragraph above), this assumption seems valid. Including these constraints with GALFIT, we derived flux densities at 350 and 500 μm for component B of $S_{350} = 56 \pm 7$ mJy and $S_{500} = 34 \pm 8$ mJy. The values for component A are a factor of 1.5 fainter (by construction). The SPIRE flux density measurements for component B are detailed in Table 1.

[9] http://herschel.esac.esa.int/twiki/bin/view/Public/SpireCalibrationWeb

In addition to the measured flux density uncertainties, SPIRE data suffer noise from confusion, for which Nguyen et al. (2010) report 1σ errors of 5.8, 6.5, and 7.3 mJy beam^{-1} for 250, 350, and 500 μm. Therefore, we adopt conservative errors, adding the flux measurement and confusion errors in quadrature, giving total flux density errors of 6.1, 9.4, and 10.5 mJy. We use these total errors when fitting the suite of models and computing IR luminosities and dust temperatures as detailed below. We also use previously published MIPS 70, SCUBA 450 and 850 μm flux densities, which for component B are 2.56 ± 0.9 mJy, 75 ± 15 mJy, and 17 ± 2 mJy, respectively (P09; Kneib et al. 2004).

3. RESULTS

3.1. Infrared Luminosity and Dust Properties

We use the *Herschel* SPIRE flux densities, *Spitzer* MIPS 70 μm data, and SCUBA 450 and 850 μm data to construct an infrared SED for component B of SMM J163554.2+661225. We fit a suite of IR SED templates from Chary & Elbaz (2001; hereafter CE01) and Dale & Helou (2002; hereafter DH02) to the combined data, finding the best-fit model via χ^2 minimization. The total L_{IR} is derived by integrating the best-fit models between 8 and 1000 μm. From the best-fit DH02 template we derive a total infrared luminosity of $6.8 \times 10^{11}\ L_{\odot}$, with a reduced $\chi^2 = 1.4$. For the best-fit CE01 template we derive a total IR luminosity of $L_{\mathrm{IR}} = 7.0 \times 10^{11}\ L_{\odot}$, with a reduced $\chi^2 = 1.2$. Both values of L_{IR} are corrected for the gravitational-lensing magnification factor of 22. Figure 2 shows the IR SED and the best-fit SED curves to the data. Figure 2 also shows the best fit to the 70, 450, and 850 μm data alone. Without the *Herschel* data the best-fit template has a peak that is shifted to longer wavelengths. To determine the uncertainty on our best-fit models we ran 10^4 Monte Carlo simulations, varying the input flux density measurements by a Gaussian random amount proportional to their errors in each simulation. The resulting 68% confidence ranges of the derived total IR luminosity from the best fits are $6.8 \pm 0.6 \times 10^{11}\ L_{\odot}$ and $7.0 \pm 0.5 \times 10^{11}\ L_{\odot}$. Combining the results from the different templates we get an average $L_{\mathrm{IR}} = 6.9 \pm 0.6 \times 10^{11}\ L_{\odot}$; thus the uncertainty on L_{IR} from the photometric data uncertainties dominates over systematic effects from the choice of models. Previous estimates of L_{IR} ranged from 5 to $10 \times 10^{11}\ L_{\odot}$ based on DH02, CE01, and Rieke et al. (2009) templates (P09), and 5.7 to $9.5 \times 10^{11}\ L_{\odot}$ based on DH02 templates (Rigby et al. 2008). Thus, the addition of the *Herschel* data results in higher accuracy and shrinks the uncertainty on L_{IR} from a factor of order two down to 10%.

The CE01 SED templates were constructed to match correlations between the observed mid-IR and FIR fluxes of local

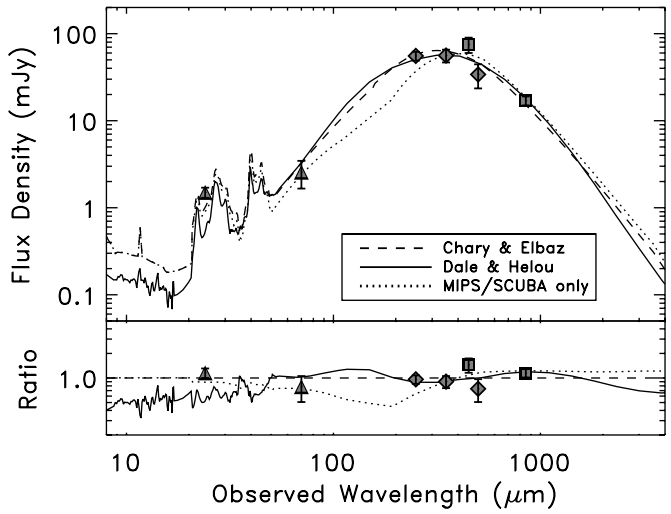

Figure 2. Infrared SED of SMM J163554.2+661225. The top panel shows flux densities from MIPS 24 and 70 μm (triangles), SPIRE 250, 350, and 500 μm (diamonds), and SCUBA 450 and 850 μm (squares) measured flux densities. All error bars on the data points are shown at 1σ. The solid and dashed curves show the IR SED template fits to the 70, 250, 350, 450, 500, and 850 μm flux densities, using templates from DH02 (solid line) and CE01 (dashed line). The *Herschel* data constrain the peak of the dust emission to shorter wavelengths compared to the best-fit CE01 template to the SCUBA and MIPS 70 μm data alone, shown by the dotted line. The bottom panel shows the ratio of the best-fit models and data points to the best-fit model of the CE01 model (to all data points). As with the top panel, the error bars are 1σ.

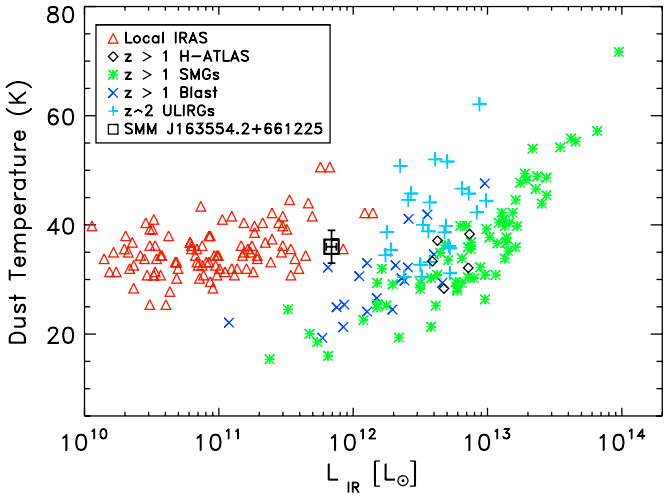

Figure 3. Total IR luminosity versus dust temperature at $z = 0$ and $z \sim 2$. SMM J163554.2+661225 is shown by the black square. The error bars shown for SMM J163554.2+661225 are 1σ. Black diamonds are $z > 1$ *Herschel*–ATLAS sources (Amblard et al. 2010); blue $\times$'s: $z > 1$ BLAST sources (Dye et al. 2009); green asterisks: $z \sim 2$ SMGs (Chapman et al. 2005); cyan crosses: $z \sim 2$ ULIRGs with *Herschel* detections (Magdis et al. 2010); and red triangles: local *IRAS*-selected galaxies with SCUBA 850 μm detections (Dunne et al. 2000).

(A color version of this figure is available in the online journal.)

galaxies. The shapes of the FIR SED of the CE01 models are calibrated on the local IR-luminosity–dust-temperature relationship. As such, the CE01 templates with higher dust temperature correspond to galaxies with higher $L_{\rm IR}$. However, we find that the shape of the FIR SED of SMM J163554.2+661225 corresponds to a much cooler dust temperature compared to local galaxies of similar luminosity. Indeed, the CE01 template that best matches the FIR SED of SMM J163554.2+661225 has an intrinsic luminosity that must be "scaled-up" by a factor of 7.5. Therefore, this best-fit template must be scaled up by a factor of nearly an order of magnitude to match both the shape of the SED and the flux density measurements of SMM J163554.2+661225. Similar results were seen by Muzzin et al. (2010) for their sample of two $z \sim 2$ galaxies, where their galaxies were comparable to local luminous FIR galaxies, but scaled up in luminosity by more than an order of magnitude. These new results confirm the conclusions of Rigby et al. (2008), and P09 who used mid- and far-IR photometry and mid-IR spectroscopy to demonstrate that SMM J163554.2+661225 is inconsistent with the spectra of local ultraluminous infrared galaxies (ULIRGs), but is consistent with the SED shape of low-$L_{\rm IR}$ local starburst galaxies and has just been "scaled-up" in luminosity and star formation by 1–2 orders of magnitude.

Using the best-fit SEDs we calculated an effective dust temperature, $T_D = 36 \pm 3$ (1σ) K, assuming a modified graybody distribution (e.g., Young et al. 1989; Calzetti et al. 2000; Amblard et al. 2010) with a fixed emissivity parameter, $\beta = 1.5$, of the form:

$$f_\nu \propto \frac{\nu^{3+\beta}}{\left[\exp\left(\frac{h\nu}{kT_D}\right) - 1\right]}. \quad (1)$$

The uncertainty on the dust temperature was derived by fitting all of the DH02 and CE01 models within 1σ of the best fit, based on the Monte Carlo simulations described above, to Equation (1).

Based on the mid-IR and SCUBA submillimeter data, P09 estimated $T_D = 52$ K. We favor the dust temperature measured here using the *Herschel* data, as these data now constrain the peak of the IR emission, providing the most constraining power on the dust temperature. The best-fit dust temperature again demonstrates that the SED shape of SMM J163554.2+661225 is not consistent with local galaxies of comparable $L_{\rm IR}$, which have significant contributions of warm ($\gtrsim$70 K) dust to the IR emission (e.g., CE01; DH02; Rieke et al. 2009).

We compare the calculated dust temperature and IR luminosity of SMM J163554.2+661225 to other galaxies that have measured dust temperatures using *Herschel* data or other submillimeter observations. Figure 3 shows T_D versus $L_{\rm IR}$ for galaxies at similar redshifts ($1 < z < 3$), including $z > 1$ sources selected from the *Herschel*–ATLAS survey (Amblard et al. 2010), $z > 1$ sources detected in BLAST (Balloon-borne Large-Aperture Submillimeter Telescope; Dye et al. 2009), $z \sim 2$ SMGs (Chapman et al. 2005), and *Herschel*-detected $z \sim 2$ ULIRGs (Magdis et al. 2010). We also compare to a sample of local *IRAS*-selected galaxies with SCUBA 850 μm detections (Dunne et al. 2000). The other samples compute $L_{\rm IR}$ (from 8 to 1000 μm) and T_D in similar ways with a fixed $\beta = 1.5$, except for the local *IRAS* sources which have varying values of β. The *IRAS* sources also quote $L_{\rm FIR}$ instead of $L_{\rm IR}$, and we converted these using $L_{\rm IR} = 1.4 \times L_{\rm FIR}$ (Dale et al. 2001). If we change β over a range of 2.0 to 1.2 for our object, then this corresponds to a range in dust temperatures of 25–42 K. However, if β is allowed to vary, the best-fit value of $\beta = 1.6$ results in $T_D = 34.5$ K, consistent with our result for a fixed $\beta = 1.5$.

In Figure 3, SMM J163554.2+661225 has a similar dust temperature to the local *IRAS* sources, almost all of which have lower $L_{\rm IR}$. It has a dust temperature that is lower than local *IRAS* sources of comparable $L_{\rm IR}$. While SMM J163554.2+661225 has a somewhat warmer dust temperature than other $z \sim$ 1–2 SMGs of comparable $L_{\rm IR}$, Chapman et al. (2005) discuss how the dust temperature of high-redshift submillimeter-selected samples are biased to cooler temperatures. Furthermore, SMM

J163554.2+661225 appears to be in a "bridge" region between IR-luminous galaxies with cool and warm dust temperatures. Magdis et al. (2010) also note that their $z \sim 2$ ULIRG sample with *Herschel* detections bridges the "cooler" high-z SMGs to the "warmer" local/intermediate-z ULIRGs.

We estimate the total dust mass using our estimate of the dust temperature and the FIR luminosity. To estimate the total dust mass in SMM J163554.2+661225, we adopt the formulation of Young et al. (1989) and Calzetti et al. (2000):

$$M_{\rm dust} = C S_{100} D^2 [\exp(143.88/T_D) - 1]\,(M_\odot), \qquad (2)$$

where S_{100} is the rest-frame flux at 100 μm in Jy, D is the distance to the galaxy in Mpc, the expression in square brackets is the temperature-dependent part of the blackbody distribution, and C is a scale factor that depends on the physical properties of the dust grains: $C \sim 6\ M_\odot\ {\rm Jy}^{-1}\ {\rm Mpc}^{-2}$ for $\beta = 2$ and $\sim 5\ M_\odot\ {\rm Jy}^{-1}\ {\rm Mpc}^{-2}$ for $\beta = 1.5$ (Young et al. 1989; Calzetti et al. 2000). For the range in single-component dust temperatures, we estimate a total dust mass for this galaxy of $2.8\ ^{+1.2}_{-0.8}\ (1\sigma) \times 10^8\ M_\odot$, corrected for the gravitational-lensing magnification factor of 22. This is approximately a factor of 10 higher than the estimated dust mass from Kneib et al. (2005) based on the 850 μm flux density and a dust temperature of ~50 K. This can be explained by the colder dust temperature determined here, as there will be a larger fraction of cold dust for this galaxy with a dust temperature of 36 K compared to 50 K, resulting in a higher total dust mass. Based on the molecular gas estimate of $4.5 \times 10^9\ M_\odot$ by Kneib et al. (2005) this implies a dust-to-gas mass ratio of 0.06. This is consistent with ratios found for local star-forming IR galaxies in the Survey of Nearby Infrared Galaxies (SINGS; Kennicutt et al. 2003; Draine et al. 2007) sample.

P09 also noted that SMM J163554.2+661225 has a lower ratio of $L(24\ \mu{\rm m})/L({\rm Pa}\alpha)$ compared to what is measured for any local ULIRGs, demonstrating that SMM J163554.2+661225 lacks a warm ($T_D \sim 70$ K) dust component. However, there could be a colder dust component present in SMM J163554.2+661225. The local samples of *IRAS*-selected galaxies (Dunne et al. 2000) preferentially detected galaxies with large amounts of $T_D > 40$ K, but because these galaxies were selected with *IRAS* they miss most of the cold-dust-dominated sources. The observations of optically selected galaxies of the SCUBA Local Universe Galaxy Survey (SLUGS; Vlahakis et al. 2005), supplemented by *Spitzer* data of a subsample of SLUGS galaxies by Willmer et al. (2009), showed that the mid-to-far-IR SEDs of these galaxies are better matched with both cold and warm dust components. These samples show on average a 2× larger proportion of cold dust relative to warm dust than solely IR-selected galaxy samples do, such as the *IRAS*-selected sample (Dunne et al. 2000) and SINGS sample (Kennicutt et al. 2003).

We fit models of Draine & Li (2007) to the SED of SMM J163554.2+661225 in order to investigate a two-component dust fit. The implied total IR luminosity from the best-fit Draine & Li model is $7.0 \times 10^{11}\ L_\odot$, consistent with our other SED fits. The best-fit Draine & Li (2007) SED is modeled with a modified graybody distribution with two dust components, each with $\beta = 1.5$. This fit corresponds to warm and cold effective dust temperatures of 46 K and 28 K. Using the dust mass equation above, we calculate warm and cold dust mass components of $M_{\rm cold} = 4.3 \times 10^8\ M_\odot$ and $M_{\rm warm} = 5.6 \times 10^7\ M_\odot$. The mass from the warm dust component more closely matches the estimated total dust mass determined by Kneib et al. (2005). The ratio of $M_{\rm cold}/{\rm M}_{\rm warm} = 7.8$, with a total dust mass $= 4.9 \times 10^8\ M_\odot$, consistent within 2σ of our result of the dust mass estimate from the single-component temperature fits. This lower ratio of cold dust to warm dust for SMM J163554.2+661225 is more similar to that of the SINGS sample than in the SLUGS sample (Draine et al. 2007; Willmer et al. 2009). The SLUGS sample typically had higher ratios of $M_{\rm cold}/M_{\rm warm}$, on order ~1000 (Willmer et al. 2009). This agrees with the result of Rigby et al. (2008) who noted the similarity between the mid-IR emission features of SMM J163554.2+661225 and that of local IR star-forming galaxies.

4. STAR FORMATION RATES AND IMPLICATIONS FOR THE IMF

Local star-forming galaxies show a tight trend between $L({\rm Pa}\alpha)$ and $L_{\rm IR}$ (e.g., Calzetti et al. 2005; Alonso-Herrero et al. 2006), both of which trace the instantaneous SFR. We calculate the SFR of SMM J163554.2+661225 based on the derived total IR luminosities from the SED fitting, using the relation derived by Kennicutt (1998), which gives ${\rm SFR} = 4.5 \times 10^{-44} \times {\rm FIR}\ ({\rm erg\ s^{-1}}) = 119 \pm 10\ M_\odot\ {\rm yr^{-1}}$ for a Salpeter IMF from 0.1 to 100 $M_\odot$. Previous estimates of SFRs from the total IR emission in this galaxy range from ${\rm SFR_{IR}} = 90$–$180\ M_\odot\ {\rm yr^{-1}}$ (P09) and ${\rm SFR_{IR}} = 140 \pm 30\ M_\odot\ {\rm yr^{-1}}$ (Rigby et al. 2008). Our estimate of the IR emission from *Spitzer*, *Herschel*, and the submillimeter is consistent with these results, although the uncertainty on our measurement is significantly reduced by including the *Herschel* far-IR data.

P09 obtained a Paα measurement of component B using *Spitzer* IRS spectroscopy with the SL2 module and measured a Paα SFR; the *Spitzer* IRS observations only covered component B, so we can only compare the IR-derived SFR to the Paα SFR for component B. P09 measured a Paα line flux for component B of $8.6 \pm 1.4 \times 10^{-16}\ {\rm erg\ s^{-1}\ cm^{-2}}$, which is uncorrected for dust attenuation and gravitational-lensing magnification. Kneib et al. (2004) measured an Hα line flux of $5.9 \times 10^{-16}\ {\rm erg\ s^{-1}\ cm^{-2}}$. We re-calculate the dust-corrected Paα luminosity, using an updated value for the dust attenuation for the Paα line (see P09). We use the ratio of the Paα line flux to the Hα line flux to estimate the amount of dust attenuation affecting the nebular gas, assuming the Calzetti et al. (2000) dust law. This results in an extinction estimate of $A(V) = 3.9 \pm 0.4$ mag and this corresponds to $A({\rm Pa}\alpha) = 0.58 \pm 0.04$ mag (we assume that the stellar continuum is attenuated at the same level as the nebular lines (e.g., Erb et al. 2006; though see also Förster Schreiber et al. 2009)). Correcting for the dust extinction and applying a gravitational-lensing magnification factor of 22, the Paα line luminosity is $L({\rm Pa}\alpha)_{\rm cor} = 3.38 \pm 0.55 \times 10^{42}\ {\rm erg\ s^{-1}}$. This corresponds to an extinction- and lensing-corrected ${\rm SFR_{Pa\alpha}} = 225 \pm 37\ M_\odot\ {\rm yr^{-1}}$, following the Kennicutt (1998) relations. This luminosity corresponds to an ionizing continuum flux of $Q_{\rm ion} = 2.1 \pm 0.3 \times 10^{55} \gamma\ {\rm s^{-1}}$. This updated dust correction results in a 30% increase in the derived Paα luminosity and Paα SFR, and $Q_{\rm ion}$ from that originally derived by P09.

Our estimate of the SFR derived from the IR emission, ${\rm SFR(IR)} = 119 \pm 10\ M_\odot\ {\rm yr^{-1}}$, is significantly different than the SFR calculated from the dust-corrected Paα line, ${\rm SFR(Pa}\alpha) = 225 \pm 37\ M_\odot\ {\rm yr^{-1}}$. They are offset by a factor of 1.9 ± 0.35, a 2.5σ discrepancy (or a 99% confidence). The offset between the SFR derived from the Paα line and IR implies that one or more of our assumptions are incorrect. We consider here several explanations to account for the apparent discrepancy between the IR and Paα SFRs.

4.1. Variations in Dust Attenuation

In our analysis, we corrected the Paα line luminosity assuming a Calzetti dust extinction law (Calzetti et al. 2000). The exact level of dust attenuation is uncertain (see below), but changes in the assumed extinction are unable to account fully for the measured offset between the IR and Paα SFRs. For example, P09 report a Paα luminosity of $2.05 \pm 0.33 \times 10^{42}$ erg s^{-1} *uncorrected* for dust extinction. This corresponds to an SFR of $130 \pm 21\ M_{\odot}$ yr^{-1}. If there is no dust extinction correction the SFRs are consistent at the 1σ level. However, zero dust attenuation seems unlikely. First, the ratio of the measured nebular emission lines is strongly inconsistent with the assumption of zero dust (see below). Second, P09 showed from modeling the rest-frame UV-to-NIR photometry of the galaxy with stellar population synthesis models (Bruzual & Charlot 2003) that the dominant star-forming component has a best fit with $A(V) \sim 3.2$ mag. Finally, the simple fact that this galaxy is bright in the far-infrared implies that it contains a significant amount of dust (see Section 3.1). Therefore, significant dust extinction seems to be required.

In our analysis, using the dust extinction law of Calzetti et al. (2000) results in a line extinction measurement of $A(\mathrm{Pa}\alpha) = 0.58$ mag derived from the observed ratio of the Hα and Paα lines. Using other dust attenuation laws (e.g., Dopita et al. 2005; Cardelli et al. 1989) results in slightly larger extinction estimates and would therefore *increase* the dust-corrected Paα luminosity by $\sim$10%. This amplifies the offset between the Paα-derived SFR and IR-derived SFR. Thus, the use of the Calzetti dust law results in a conservative estimate of the Paα luminosity and $\mathrm{SFR}_{\mathrm{Pa}\alpha}$, and therefore minimizes the differences between the two SFR measurements.

The Paα dust extinction determined above is based on the ratio of the Hα line flux from Kneib et al. (2004) to the Paα line flux. However, there are some discrepancies in the reported Hα line flux measurement, and it could be as much as 4$\times$ fainter (P09; W. Rujopakarn et al. 2011, in preparation), but a fainter Hα line flux would image a *larger* derived $A(V)$ and $A(\mathrm{Pa}\alpha)$, and would increase the extinction-corrected Paα luminosity and SFR (e.g., a Hα line flux lower by a factor of four would increase the dust-corrected Paα line flux by $\sim$30%).

We also we re-calculate $A(\mathrm{Pa}\alpha)$ using a newer measurement of Hβ for this galaxy from Richard et al. (2011). The observed Paα line flux for this galaxy again is $8.6 \pm 1.4 \times 10^{-16}$ erg s^{-1}, uncorrected for the gravitational-lensing magnification or dust attenuation (P09). The observed Hα line flux for component B (making no correction for uncertainties in gravitational lensing, dust attenuation, or slit losses) is 5.9×10^{-16} erg s^{-1} (Kneib et al. 2004), and the Hβ line flux is $6.88 \pm 0.29 \times 10^{-17}$ erg s^{-1} (Richard et al. 2011). Given these three lines we calculate an average $E(B-V)$ of 0.97 ± 0.07 and this corresponds to an average $A(\mathrm{Pa}\alpha)$ of 0.57 ± 0.06 assuming the Calzetti et al. (2000) attenuation law. Therefore, the addition of the Hβ line confirms the estimate of the dust attenuation affecting the nebular gas, and implies the extinction is approximately optically thin to these photons.

Lastly, the extinction correction derived here assumes the nebular gas is approximately optically thin to photons from Hα and Paα. While this is supported by the measured line ratios, if the opacity of the nebular gas is substantially higher, then it will obscure a higher fraction of emission associated with star formation. However, if this is the case, then the $A(\mathrm{Pa}\alpha)$ we derive above is only lower limit, as it is only sensitive to the outermost layer of the gas. If this is the case, then the dust-corrected Paα luminosity will also be *higher*, which further exacerbates the problem.

Therefore, in summary it seems unlikely that assumptions about the dust law or the measurements of the dust attenuation of the Paα line contribute significantly to the observed offset between the IR and Paα SFRs. Indeed, our assumptions about the dust attenuation are mostly conservative and the intrinsic Paα may be larger than reported here.

4.2. Variations to the ISM Conditions

The calculations above depend on intrinsic line ratios assuming Case B recombination at $T_e = 10^4$ K. We also consider how changes in the assumed ISM temperatures affect the estimation of $A(\mathrm{Pa}\alpha)$, and therefore the derived Paα luminosity. Increasing the interstellar medium (ISM) temperature to larger values ($T_e = 2 \times 10^4$ K), as could be expected for a highly star-forming galaxy, increases the intrinsic value of Hα / Paα from 8.46 to 9.68 (Osterbrock 1989). This increases the estimated value of $A(\mathrm{Pa}\alpha)$ to 0.62 mag, an increase of 10%. This would slightly increase the dust-corrected values of $L(\mathrm{Pa}\alpha)$ and $\mathrm{SFR}_{\mathrm{Pa}\alpha}$.

As an extreme case, $A(\mathrm{Pa}\alpha)$ would be reduced to 0.46 mag if one assumes Case A recombination and a very low ISM temperature of $T_e = 2500$ K. This would decrease $L(\mathrm{Pa}\alpha)_{\mathrm{cor}}$ and $\mathrm{SFR}_{\mathrm{Pa}\alpha}$ by a maximum of 12%, but it is insufficient to account for the factor of $\sim$2 difference between the Paα and IR SFRs. Therefore, our assumption of Case B recombination with an ISM temperature of 10^4 K does not affect our conclusions.

4.3. Changes to the Star Formation History

The offset between the two SFRs could also be due to assumptions about the stellar population of SMM J163554.2+661225. The Paα and L_{IR} SFR calibrations both assume a constant SFR and a stellar population age of 100 Myr, as well as a Salpeter IMF. Using the 2007 version of the Bruzual & Charlot (2003) stellar population synthesis models, we investigated if this factor of 1.9 between the derived SFRs could be accounted for by varying the SFH or age, but still with a Salpeter IMF. For example, the commonly assumed relations of Kennicutt (1998) assume a roughly constant SFH for the past 100 Myr. However, there is evidence that galaxies at $z > 2$ have SFHs that increase with time (e.g., Papovich et al. 2011), which affects the relative proportion of stars that contribute to nebular emission and the IR emission.

From the stellar population synthesis models with a Salpeter IMF, we calculate the ratio of ionizing photons (Q_{ion}) to bolometric luminosity versus stellar population age. We assume that the ratio of $Q_{\mathrm{ion}}/L_{\mathrm{bol}}$ is proportional to the ratio of Paα luminosity to total IR luminosity (as argued by Kennicutt 1998). We tested how an SFR that rises with time affects the ratio of $Q_{\mathrm{ion}}/L_{\mathrm{bol}}$. Assuming the SFR rises with time (approximated by the delayed SFR model within Bruzual & Charlot 2003), we find a maximal increase of $Q_{\mathrm{ion}}/L_{\mathrm{bol}}$ by at most a factor of 1.25 compared to this ratio for constant SFR. Other increasing SFRs (including a model with exponentially increasing SFR) were also investigated which produce more Lyman-continuum photons by as much as a factor of 1.3 for ages $\lesssim$ a few e-folding times. Higher ratios are possible, but only in extreme situations, such as exponentially increasing SFRs at ages $\gg$ a few e-folding times, but it seems physically unlikely that a galaxy will increase its SFR exponentially for such sustained periods without disruption (i.e., feedback). Therefore, SFH alone can only partially explain the offset between the two derived SFRs.

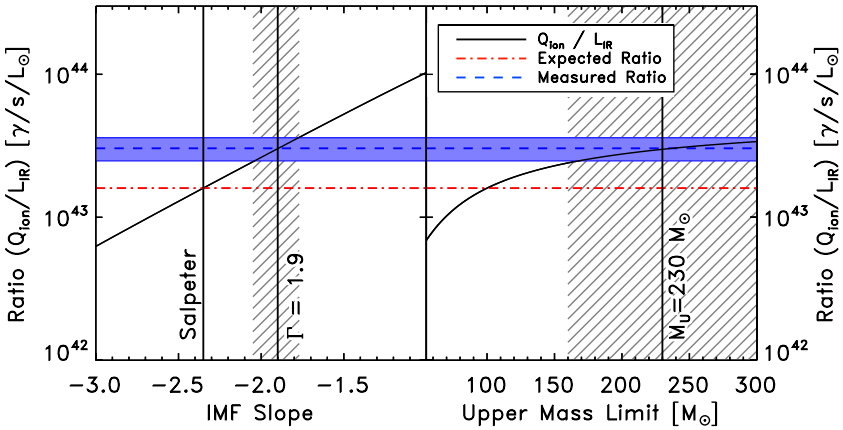

Figure 4. Effect of changes to the IMF on the ratio of the number of ionizing photons ($Q_{\rm ion}$) to $L_{\rm IR}$. Both scenarios or a combination can reproduce the measured difference between the $\rm SFR_{IR}$ and $\rm SFR_{Pa\alpha}$. The left plot shows how varying the IMF slope changes the derived ratio of $Q_{\rm ion}$ to $L_{\rm IR}$. The red dot-dashed line shows the expected ratio following the Kennicutt relations assuming a Salpeter mass distribution with upper and lower mass cutoffs of 100 $M_\odot$ and 0.1 $M_\odot$. The blue dashed line shows our measured value of $Q_{\rm ion}$ / $L_{\rm IR}$ and the blue shaded area shows the 1σ uncertainty on the measured ratio. To match our observations, more ionizing photons need to be made relative to the $L_{\rm IR}$ (traced by the bolometric luminosity; see Kennicutt 1998) which can happen with a shallower IMF distribution with slope $\Gamma = 1.9 \pm 0.15$. The right plot shows that we can also reproduce our observed ratio of $Q_{\rm ion}/L_{\rm IR}$ with a Salpeter IMF by extending the upper mass limit to 200 $M_\odot$. The gray hatched region in each panel shows our preferred 1σ values.

(A color version of this figure is available in the online journal.)

4.4. Varying the IMF

One possible way to create more ionizing photons would be an IMF that is weighted toward high-mass stars compared to that of an IMF with a Salpeter-like IMF slope. We investigated how changes in the form of the IMF affects the $Q_{\rm ion}/L_{\rm bol}$ ratio, including an IMF with a flatter slope (i.e., a "top-heavy" IMF) or an IMF with a higher upper mass cutoff. The expected ratio of the total number of ionizing photons ($Q_{\rm ion}$) to the total IR luminosity, $Q_{\rm ion}/L_{\rm IR}$, following the Kennicutt (1998) relations and assuming a Salpeter IMF from 0.1 to 100 $M_\odot$, should have a ratio of 1.6×10^{43} γ s^{-1} $L_\odot{}^{-1}$. This assumes that the Paα-derived SFR and the IR-derived SFR should be equal. However, our measured ratio for SMM J163554.2+661225 is $Q_{\rm ion}/L_{\rm IR}$ is $3.0 \pm 0.6 \times 10^{43}$ γ s^{-1} $L_\odot{}^{-1}$, reflecting the factor of 1.9 difference between the two SFRs compared to the theoretical value.

We computed $Q_{\rm ion}$ and $L_{\rm IR}$ (assumed to be $\sim L_{\rm bol}$) as a function of both the IMF slope and upper mass cutoff. To make this calculation, we take empirical measures of Q_0 as a function of spectral type for O stars with masses 19.3–100 $M_\odot$ derived by Sternberg et al. (2003).[10] We then weighted the values by the number of stars per unit mass for each IMF and integrate to calculate the total number of ionizing photons for a given IMF. We repeated the calculation for the bolometric luminosity, assuming a mass–luminosity relation of $L \propto M^{3.8}$ for stars less than 20 $M_\odot$ (Popper 1980), and $L \propto M^{1.9}$ for $M > 20$ $M_\odot$ based on empirical models of OB stars (Sternberg et al. 2003).

Figure 4 shows the effect on the ratio $Q_{\rm ion}/L_{\rm IR}$ for IMFs of different forms, including changes in the IMF slope and the upper mass cutoff. We have overplotted both the expected ratio from Kennicutt (1998) and our measured ratio. The left panel shows that a shallower IMF slope, with a best fit of $\Gamma = 1.9 \pm 0.15$, reproduces our measured ratio of $Q_{\rm ion}/L_{\rm IR}$. This result is a 3σ variation from Salpeter ($\Gamma = 2.35$). As shown in the right panel, a Salpeter IMF slope with an upper mass cutoff extended up to $\sim$200 $M_\odot$ also reproduces the measured ratio. The 1σ uncertainty on the measured ratio of $Q_{\rm ion}/L_{\rm IR}$ is also shown in Figure 4 by the blue shaded area. The vertical hatched region in each panel shows our preferred 1σ values. Therefore, a flattening of the IMF slope to $\Gamma = 1.9 \pm 0.15$ or an increase in the IMF upper mass cutoff to at least 160 $M_\odot$ (or a combination of both) is able to account for the observed Paα line luminosity and IR luminosity.

P09 estimate that SMM J163554.2+661225 has a total stellar mass of $\sim 10^{10}$ $M_\odot$. This implies that the total number of O stars ($M \geqslant 20$ $M_\odot$) is about 10^7, assuming a Salpeter IMF from 0.1 to 100 $M_\odot$ and a constant SFR. If the IMF slope varies from the nominal value of Salpeter to $\Gamma = 1.9$ then the number of O stars between 20 and 100 $M_\odot$ would increase by a factor of 3.5. Alternatively, this additional number of O stars can be accounted for by extending the upper mass cutoff to at least 160 $M_\odot$; this would result in $\sim$5% more O stars above 100 $M_\odot$, in which case the majority of the additional ionization comes from these highest mass stars.

4.5. Metallicity Effects

We also investigate if changes in metallicity can account for the measured discrepancy in the SFRs. In the above calculations for a varying SFH or a changing IMF, we assume solar metallicity. Using stellar population synthesis models from Starburst 99 (Leitherer et al. 1999), we specifically try to determine if lower metallicities can reproduce the observed ratio of $Q_{\rm ion}/L_{\rm bol}$. We ran four simulations in Starburst 99, only varying the metallicity. In all four simulations, we assumed a constant SFR of 120 $M_\odot$ yr^{-1} and a Salpeter IMF between 0.1 and 100 $M_\odot$. The four simulations had metallicities of 0.02 $Z_\odot$, 0.2 $Z_\odot$, 0.4 $Z_\odot$, and solar metallicity. Based on these results, we found that the simulation with solar metallicity at an age of 100 Myr reproduces the expected ratio of the number of ionizing photons to $L_{\rm bol}$ (1.6×10^{43} ionizing γ s^{-1} $L_\odot{}^{-1}$) as calculated following the Kennicutt (1998) relations as described above. This is the factor of 1.9 lower than our measured ratio of $Q_{\rm ion}/L_{\rm bol}$. In order to reproduce our measured ratio of $Q_{\rm ion}/L_{\rm bol}$, the metallicity must be lowered to $\lesssim$0.02 $Z_\odot$. Therefore, a very low metallicity population could reproduce the

[10] We assume that Q_0 increases with stellar mass at a rate derived from the empirical measurements of Sternberg et al. (2003). We extrapolated this rate to estimate Q_0 values above 100 $M_\odot$.

higher rate of ionizing photons as compared to the total luminosity without changing the IMF.

However, we have reason to believe that the metallicity of this galaxy is nearly solar. Using the line ratios of [N II]/Hα = 0.3 ± 0.1 (Kneib et al. 2004) and [O III]/Hβ = 1.5 ± 0.11 (Richard et al. 2011), we calculate the metallicity based on the N2 and O3N2 indices. From the N2 index, we get a value of 12 + log(O/H) = 8.6 ± 0.1, assuming the relation from Pettini & Pagel (2004), consistent with the solar value 12 + log(O/H) = 8.66. From the O3N2 index, we get a value of 8.5 ± 0.06, again close to solar metallicity. Therefore, the gas metallicity of SMM J163554.2+661225 appears to be consistent with solar metallicity and is inconsistent with a metallicity of 0.02 $Z_{\odot}$ by more than 4σ. Since they have just formed, we can also expect the massive OB stars that produce the increased fraction of ionizing photons to have a similar metallicity as the gas, and therefore it is not likely that a very low metallicity stellar population is responsible for the high measured value of $Q_{\rm ion}/L_{\rm bol}$.

4.6. Differential Magnification

As a final possibility for a cause of the differing SFRs we look at the lensing model of SMM J163554.2+661225 in order to determine if there is evidence for differential magnification between the physical region of the galaxy that produces the Paα emission relative to the IR-producing regions. For example, if Paα- and IR-emitting regions have different gravitational-lensing magnification factors, then this could contribute to the discrepancies we observe.

The gravitational-lensing model at the astrometric position of the galaxy shows variations in magnification of order 10%–20% over the 1 arcsec scale of the galaxy (J.-P. Kneib 2011, private communication), and this could contribute to the measured offset. However, it seems more likely that the Paα- and IR-emitting regions are co-aligned. We note that the *Spitzer*/IRAC data and MIPS 24 μm centroids are aligned to better than 1 arcsec, suggesting the regions contributing to the emission at these wavelengths are magnified equally. Therefore, while we cannot exclude that variations in gravitational lensing contribute, we argue that it is unlikely to dominate the measured offset.

5. SUMMARY AND FINAL THOUGHTS

The *Herschel* SPIRE data of SMM J163554.2+661225 allow for a highly accurate fit to the infrared SED of this $z = 2.515$ lensed galaxy. We measured a best-fit IR luminosity of 6.9 ± 0.6 × 10^{11} $L_{\odot}$, corresponding to a dust temperature of 36 ± 3 K, and a dust mass of ∼3 × 10^{8} $M_{\odot}$. The IR-derived SFR is 119 ± 10 $M_{\odot}$ yr^{-1} which is a factor of 1.9 lower than the previously derived Paα SFR. In order to account for the discrepancy in the derived SFRs, we have analyzed several different scenarios that could alter the ratio of Paα luminosity and $L_{\rm IR}$. One possibility is that there is a varying SFH due to a rising SFR. Using an SFR that increases with time with a Salpeter IMF can increase the number of ionizing photons relative to the total bolometric luminosity (and thereby to the $L_{\rm IR}$), by as much as 25%–30% at a given stellar population age, but cannot by itself account for the measured difference between $\rm SFR_{IR}$ and $\rm SFR_{Pa\alpha}$.

Varying the high-mass end of the IMF can explain our results, either by increasing the high mass cutoff up to at least 160 $M_{\odot}$, or changing the IMF slope to $\Gamma = 1.9$ from the Salpeter value of $\Gamma = 2.35$, or a combination of the two. Either scenario produces an increase in the number of massive stars, resulting in higher rates of ionizing photons. This appears necessary to explain the higher Paα-derived SFR over the IR-derived SFR. However, with current data we are unable to distinguish between these two scenarios. Similar changes in the IMF at the high-mass end have been shown to have an effect on the relative contributions between various SFR indicators (e.g., Daddi et al. 2007), whereas extending the IMF upper mass limit up to at least 120 $M_{\odot}$ has also been shown to be important in reproducing the observed Hα flux in star-forming galaxies from the SDSS (Hoversten & Glazebrook 2008, 2011). Based on our analysis, we favor a scenario where the IMF may require minor adjustments to the standard form of the Salpeter IMF for some star-forming galaxies.

Flattening of the IMF at higher redshifts has been proposed by other studies to account for offsets between stellar mass and SFR densities (e.g., Davé 2008, and references therein). A flat IMF, with $\Gamma = 1$, has also been proposed to account for SMG number counts (Baugh et al. 2005; Lacey et al. 2008). Our results of SMM J163554.2+661225 allow for an IMF slope $\Gamma = 1.9 \pm 0.15$, only slightly flatter than Salpeter. Additionally, it could be that both a slight change in the IMF and a change to the SFH are at play. If the SFH is changing or there has been a burst in star formation activity, this could mimic some of the changes produced via a varying IMF. However, a more complex SFH only cannot explain the whole effect we see; some alteration of the IMF is still needed. As discussed above, if the galaxy has an SFR that is increasing with time, then this would increase the expected number of ionization photons by 25% compared to a constant SFR. In this case, coupled with the increasing SFR, then the IMF would only be slightly flatter than Salpeter with a slope $\Gamma \sim 2.06$ and/or with an upper mass cutoff of up to 120 $M_{\odot}$.

We also investigated if changes to the assumed metallicity and dust content of this galaxy could account for the offset in derived SFRs. This galaxy would need a very low metallicity population of ∼0.02 $Z_{\odot}$; however this low metallicity does not match with the observed line ratios of the gas, which give a measured metallicity of ∼ solar. A lower dust extinction of $A(V) = 1.0$ mag, corresponding to $E(B - V) = 0.25$ mag, and $A(\rm Pa\alpha) = 0.15$ mag could also account for the discrepancy between the IR-derived and Paα-derived SFRs. However, changing the assumptions about the ISM conditions (i.e., temperature or Case A versus Case B recombination) only has a small effect on the derived $A(V)$ values for this galaxy, and at most can only decrease the derived Paα SFR by 12%, again not enough to make up the difference between the two SFRs. Also from stellar population synthesis modeling, previous authors (P09) have shown that this galaxy is best fitted by a two-component stellar population fit, with the dominant star-forming component being very dusty, corresponding to $E(B - V) = 0.8$ mag and $A(V) \sim 3.2$, and therefore inconsistent with $A(V) \sim 1$. We therefore conclude that the assumptions we have made about the metallicity and dust content of this galaxy are consistent with the known observations of this galaxy, and it would take extreme changes to one or the other in order to be able to explain the differences in the derived SFRs.

Another possibility to explain the offset is that the regions of the galaxy that emit the Paα and IR may experience different amounts of gravitational-lensing magnification. However, we expect the Paα emission to trace the star-forming and IR-dominated regions. Given the size of the galaxy, this effect seems to be less than ≈20%, and likely is not a dominant effect.

As a final thought, it may be that a combination of all the effects (variations in the SFH, minor adjustments to the IMF, variations in extinction, etc.) may all contribute to the difference in the Paα-derived SFR and the IR SFR. Future observations of $z \sim 2$ lensed galaxies that have both Paα emission and FIR observations may be able to determine if this offset is common at $z \sim 2$ or if SMM J163554.2+661225 is an unusual case.

The authors wish to thank Kim-Vy Tran for many useful conversations, Jean-Paul Kneib for his help on questions regarding the lensing model, as well as Rob Ivison and Anthony Smith for help with questions regarding the HerMES survey. We also thank the anonymous referee for a very useful report which improved the quality of this paper. This research has made use of data from HerMES project (Oliver et al. 2010; http://hermes.sussex.ac.uk/). HerMES is a Herschel Key Programme utilizing Guaranteed Time from the SPIRE instrument team, ESAC scientists, and a mission scientist. The HerMES data were accessed through the HeDaM database (http://hedam.oamp.fr) operated by CeSAM and hosted by the Laboratoire d'Astrophysique de Marseille. This work is based in part on observations made with the *Herschel Space Observatory* and the *Spitzer Space Telescope*, which is operated by the Jet Propulsion Laboratory, California Institute of Technology under a contract with NASA. Support for this work was provided by NASA through an award issued by JPL/Caltech. Further support for K.D.F., C.P., and S.L.F. was provided by Texas A&M University. S.L.F. also received support by NASA through Hubble Fellowship Grant HST-HF-51288.01, awarded by the Space Telescope Science Institute, which is operated by the Association of Universities for Research in Astronomy, Inc., for NASA, under contract NAS 5-26555.

REFERENCES

Alonso-Herrero, A., Rieke, G. H., Rieke, M. J., et al. 2006, ApJ, 650, 835
Amblard, A., Cooray, A., Serra, P., et al. 2010, A&A, 518, L9
Baldry, I. K., & Glazebrook, K. 2003, ApJ, 593, 258
Baugh, C. M., Lacey, C. G., Frenk, C. S., et al. 2005, MNRAS, 356, 1191
Bertin, E., & Arnouts, S. 1996, ApJS, 117, 393
Bruzual, G., & Charlot, S. 2003, MNRAS, 344, 1000
Calzetti, D., Armus, L., Bohlin, R. C., et al. 2000, ApJ, 533, 682
Calzetti, D., Kennicutt, R. C., Jr., Bianchi, L., et al. 2005, ApJ, 633, 871
Cardelli, J. A., Clayton, G. C., & Mathis, J. S. 1989, ApJ, 345, 245
Chapman, S. C., Blain, A. W., Smail, I., & Ivison, R. J. 2005, ApJ, 622, 772
Chapman, S. C., Scott, D., Borys, C., & Fahlman, G. G. 2002, MNRAS, 330, 92
Chary, R., & Elbaz, D. 2001, ApJ, 556, 562 (CE01)
Daddi, E., Dickinson, M., Morrison, G., et al. 2007, ApJ, 670, 156
Dale, D. A., & Helou, G. 2002, ApJ, 576, 159 (DH02)
Dale, D. A., Helou, G., Contursi, A., Silbermann, N. A., & Kolhatkar, S. 2001, ApJ, 549, 215
Davé, R. 2008, MNRAS, 385, 147
Dopita, M. A., Groves, B. A., Fischera, J., et al. 2005, ApJ, 619, 755
Draine, B. T., Dale, D. A., Bendo, G., et al. 2007, ApJ, 663, 866
Draine, B. T., & Li, A. 2007, ApJ, 657, 810
Dunne, L., Eales, S., Edmunds, M., et al. 2000, MNRAS, 315, 115
Dye, S., Ade, P. A. R., Bock, J. J., et al. 2009, ApJ, 703, 285
Elbaz, D., Hwang, H. S., Magnelli, B., et al. 2010, A&A, 518, L29
Elmegreen, B. G. 2006, ApJ, 648, 572
Erb, D. K., Steidel, C. C., Shapley, A. E., et al. 2006, ApJ, 647, 128
Fazio, G. G., Hora, J. L., Allen, L. E., et al. 2004, ApJS, 154, 10
Finkelstein, S. L., Rhoads, J. E., Malhotra, S., Pirzkal, N., & Wang, J. 2007, ApJ, 660, 1023
Förster Schreiber, N. M., Genzel, R., Bouché, N., et al. 2009, ApJ, 706, 1364
Gouliermis, D., Brandner, W., & Henning, Th. 2005, ApJ, 623, 846
Griffin, M. J., Abergel, A., Abreu, A., et al. 2010, A&A, 518, L3
Houck, J. R., Roellig, T. L., van Cleve, J., et al. 2004, ApJS, 154, 18
Hoversten, E. A., & Glazebrook, K. 2008, ApJ, 675, 163
Hoversten, E. A., & Glazebrook, K. 2011, in ASP Conf. Ser. 440, UP2010: Have Observations Revealed a Variable Upper End of the Initial Mass Function?, ed. M. Treyer et al. (San Francisco, CA: ASP), 251
Kennicutt, R. C. 1998, ARA&A, 36, 189
Kennicutt, R. C., Armus, L., Bendo, G., et al. 2003, PASP, 115, 928
Kneib, J.-P., Neri, R., Smail, I., et al. 2005, A&A, 434, 819
Kneib, J.-P., van der Werf, P. P., Kraiberg Knudsen, K., et al. 2004, MNRAS, 349, 1211
Kudritzki, R.-P., Méndez, R. H., Feldmeier, J. J., et al. 2000, ApJ, 536, 19
Lacey, C. G., Baugh, C. M., Frenk, C. S., et al. 2008, MNRAS, 385, 1155
Lee, H.-C., Gibson, B. K., Flynn, C., Kawata, D., & Beasley, M. A. 2004, MNRAS, 353, 113
Leitherer, C., Schaerer, D., Goldader, J. D., et al. 1999, ApJS, 123, 3
Lowenstein, M., & Mushotzky, R. F. 1996, ApJ, 466, 695
Magdis, G. E., Elbaz, D., Hwang, H. S., et al. 2010, MNRAS, 409, 22
Malhotra, S., & Rhoads, J. 2002, ApJ, 565, 71
Muzzin, A., van Dokkum, P., Kriek, M., et al. 2010, ApJ, 725, 742
Nguyen, H. T., Schulz, B., Levenson, L., et al. 2010, A&A, 518, L5
Oliver, S. J., Wang, L., Smith, A. J., et al. 2010, A&A, 518, L21
Osterbrock, D. E. 1989, Astrophysics of Gaseous Nebula and Active Galactic Nuclei (Mill Valley, CA: Univ. Science Books)
Papovich, C., Finkelstein, S. L., Ferguson, H. C., Lotz, J. M., & Giavalisco, M. 2011, MNRAS, 412, 1123
Papovich, C., Rudnick, G., Rigby, J. R., et al. 2009, ApJ, 704, 1506 (P09)
Peng, C. Y., Ho, L. C., Impey, C. D., & Rix, H.-W. 2010, ApJ, 139, 2097
Pettini, M., & Pagel, B. E. J. 2004, MNRAS, 348, 59
Pilbratt, G. L., Riedinger, J. R., Passvogel, T., et al. 2010, A&A, 518, L1
Popper, D. M. 1980, ARA&A, 18, 115
Renzini, A., Ciotti, L., D'Ercole, A., & Pellegrini, S. 1993, ApJ, 419, 52
Richard, J., Jones, T., Ellis, R., et al. 2011, MNRAS, 413, 643
Rieke, G. H., Alonso-Herrero, A., Weiner, B. J., et al. 2009, ApJ, 692, 556
Rieke, G. H., Young, E. T., Engelbracht, C. W., et al. 2004, ApJS, 154, 25
Rigby, J. R., Marcillac, D., Egami, E., et al. 2008, ApJ, 675, 262
Salpeter, E. E. 1955, ApJ, 121, 161
Sternberg, A., Hoffmann, T. L., & Pauldrach, A. W. A. 2003, ApJ, 599, 1333
Vlahakis, C., Dunne, L., & Eales, S. 2005, MNRAS, 364, 1253
Willmer, C. N. A., Rieke, G. H., Le Floc'h, E., et al. 2009, AJ, 138, 146
Young, J. S., Xie, S., Kenney, J. D. P., & Rice., W. L. 1989, ApJS, 98, 219